Polymer 51 (2010) 5846–5856

Contents lists available at ScienceDirect

Polymer

journal homepage: www.elsevier.com/locate/polymer

Physical and mechanical properties of poly(methyl methacrylate) -functionalized graphene/poly(vinylidine fluoride) nanocomposites: Piezoelectric β polymorph formation

Rama K. Layek, Sanjoy Samanta, Dhruba P. Chatterjee, Arun K. Nandi*

Polymer Science Unit, Indian Association for the Cultivation of Science, Jadavpur, Kolkata 700 032, India

ARTICLE INFO

Article history:
Received 2 August 2010
Received in revised form
20 September 2010
Accepted 27 September 2010
Available online 18 October 2010

Keywords:
Graphene
Mechanical property
Conductivity

ABSTRACT

Poly(methyl methacrylate) -functionalized graphene (MG) is prepared from graphene oxide (GO), using atom transfer radical polymerization (ATRP) and reducing with hydrazine hydrate. PMMA causes an increase of height of MG sheet for polymerization of MMA at side and basal planes. MG layers become thinner for exfoliation during composite formation. Graphene sheets enhance piezoelectric β-polymorph PVDF formation. MG sheets nucleate PVDF crystals and a gradual decrease of α phase occurs with a concomitant rise of β phase. Thermal stability of nanocomposites increases significantly and the T_g increase is really large (21 °C). Storage modulus shows an increase of 124%, stress at break 157% and Young's modulus 321% for 5% MG. Parallel orientation of graphene sheets changes to random orientation for high graphene content. It exhibits conducting percolation threshold at 3.8% MG and variable range hopping model suggests that conductivity is contributed from the intergrain tunnelling and hopping between the grains.

1. Introduction

Graphene, a two dimensional carbon nanostructure has recently attracted considerable research attention for developing nanocomposites, sensors, supercapacitors, hydrogen storage, nanoelectronics and batteries [1]. Graphene has high mechanical strength [2], good biocompatibility [3], superior transport properties and giant thermoelectric properties [4]. Judicious incorporation of graphene in the polymer matrix by uniform dispersion and fine interface control may lead to the formation of high performance composites. But the difficulty in preparation of processible graphene sheets hinders the growth of it's applications. Hence, an increase of research activity for the preparation of dispersible graphene is prevailing in recent literature. There are two possible ways (physical and chemical) to produce dispersible graphene sheets. In the physical method the thermal expansion of graphite followed by ultrasonication in aqueous medium is used to disperse graphene sheets [5,6], while in the latter method chemical oxidation/reduction technique is used to obtain the dispersible graphene sheets [7–9]. The extent of thermal expansion depends on the intercalation procedure and it dictates the thickness of the graphite nanoplatelets. In the chemical procedure, introduction of a gas producing chemical reaction within its interlayer galleries cause chemical expansion of the gallery [10]. The graphene oxide (GO) route is most important in the chemical method to expand the gallery as water molecule can easily intercalate into the gallery due to the hydrophilic nature of epoxide and –OH groups produced in the oxidation. This graphene oxide after exfoliation in the medium is reduced with hydrazine or with sodium borohydride to obtain electrically conducting graphene sheets [8,9]. Such graphene sheets are usually used to produce conducting and high performance nanocomposites with commodity polymers.

In literature, there are some reports of polymer–graphene nanocomposites [11–18]. Stankovich et al. reported polystyrene–graphene nanocomposite showing the lowest percolation threshold of 0.1%(v/v) for room temperature electrical conductivity amongst the different carbon nanostructures and exhibits 10^{-3} S/cm conductivity, sufficient for many electrical applications at only 1% (v/v) of graphene [11]. A stable dispersion of polymer coated graphene by reduction of graphene oxide in presence of poly (sodium 4-styrene sulfonate) is also prepared by the same group [12]. The PMMA graphene nanocomposites [13], exhibits dramatic increase in modulus, ultimate strength and thermal stability, which are comparable to that of single walled carbon nanotube composites. The composites also exhibit a sharp rise in glass transition temperature. Recently flash irradiation technique for

* Corresponding author. Tel. +91 33 24734971; fax: +91 33 24732805.
E-mail address: psuakn@mahendra.iacs.res.in (A.K. Nandi).

0032-3861/$ – see front matter © 2010 Elsevier Ltd. All rights reserved.
doi:10.1016/j.polymer.2010.09.067

deoxygenation of graphene oxide is used to convert an insulating GO conducting [14]. However, in the epoxy resin/graphite nanocomposite the electrical conductivity has increased significantly (12 order) [15]. An addition of 2.5%(v/v) of graphene within it causes a significant loss of tensile strength, impact strength and elongation at break due to the lack of interfical adhesion. Polystyrene sulfonate stabilized graphene sheets and poly(vinyl alcohol) mixtures on ice segregation-induced self assembly (ISISA) produce three dimensional porous structure suitable for application in next generation electronic components [16]. High conductivity is achieved using latex based technology of composite formation of graphene (1.6 wt%) in polystyrene [17] Recently Prasad et al. observed synergy in the mechanical property enhancement of poly (vinyl alcohol) composite with mixture of two different carbon nanomaterials [18a]. In the polyester/exfoliated graphite nanocomposites electrical percolation data compared well with the rigidity percolation from rheological measurements [18b]. Thus research on graphene–polymer nanocomposites has gained considerable momentum to increase the mechanical property for household applications and to induce conductivity in the composite for application in electronics.

Poly(vinylidene fluoride) (PVDF) is an important polymer having piezo and pyroelectric properties. It exhibits five different crystalline polymorphic structures (α, β, γ, δ, ϵ) of which β polymorph is piezoelectrically active [19]. This polymer is about 50% crystalline and it crystallizes in the stable α polymorph from the melt. PVDF is a biocompatible polymer [20], so its composites with graphene would be very much useful for biomedical applications. In the nanocomposite of PVDF with clay [21], Ag nanoparticle [22], or carbon nanotube [23], β polymorph is produced in the solvent cast samples but a mixture of α & β polymorph is always produced in the composite quenched from the melt. In a recent report on the nanocomposites of PVDF with exfoliated graphene (EG) and with functionalized graphene sheet (FG) pure α and a mixture of α & β polymorphs are produced with the former and the later, respectively [24]. So it would be interesting if the β PVDF can be fully generated in the graphene PVDF nanocomposites. Graphene is not highly interactive with PVDF which has a strong affinity with the ester >C═O group [25]. Though insulating GO has some −COOH group it is not dispersible in DMF [26], and it does not interact with PVDF. So, in the present work we have used poly (methyl methacrylate) (PMMA) modified graphene (MG) as PMMA is highly miscible with PVDF and both are soluble in DMF [27]. The strong dipolar interaction between MG and PVDF through >C═O group of PMMA and $>CF_2$ group of PVDF [25,27], may lead to a homogenous distribution of graphene in the composite, so a significant enhancement in mechanical property is expected. In this manuscript we delineate the dispersion of MG sheets from AFM study and we have discussed the mechanical properties of this interesting material from the distribution of MG sheets in the composite. The cause of piezoelectric β polymorph formation and a mechanism of electrical conduction in this biocompatible composite are also delineated.

2. Experimental section

2.1. Samples

Graphite (Aldrich, USA), sodium nitrate and potassium permanganate (Merck, Mumbai) are used as received. Pyridine (Merck, Mumbai) is vaccum distilled before use. 2-bromoisobuyl bromide (BIB Aldrich, USA) N, N, N, N, N pentamethyl diethelene triamine (PMDETA, Aldrich) are used as received. N, N dimethyl formamide (DMF) (Rankem, New Delhi) and methyl methacrylate (MMA, Loba chemicals) are distilled in vacuum before use. CuCl (Aldrich, USA) is purified by washing with 10% HCl followed by methanol and diethyl ether in a schlenk tube under nitrogen atmosphere. Hydrazine hydrate solution (99%, synthetic grade, Merck, Mumbai) is used as received. Chloroform (Renkem, New Delhi, analytical grade) is used as received. PVDF (Aldrich, USA, $\overline{M}_n = 7.0 \times 10^4$, polydispersity index 2.57, head to head defect = 4.33 mol%) [28], is purified by recrystallization from its 0.2% (w/w) solution of acetopheneone.

2.2. Modification of graphene

Graphene oxide (GO) is prepared from graphite powder by oxidizing with $KMnO_4/NaNO_3$ mixture in concentrated H_2SO_4 medium using Hummers method [29]. In an inert reaction vessel (nitrogen atmosphere) 250 mg GO is mixed with 15 ml pyridine and the GO is dispersed by sonication. Then BIB is added slowly at 0 °C and the reaction is continued for 3 h at 0 °C and then for 24 h at 30 °C. The product is collected by repeated washing and centrifugation with water. Finally the BIB attached graphene (BIBG) is obtained and it is vacuum dried at 40 °C for two days.

To prepare graphene oxide-polymethyl methacrylate (GOPMMA) in an inert reaction vessel 100 mg BIBG, 10 mg CuCl, 20.4 μl PMDETA and 1 ml DMF are taken and purged with nitrogen gas and sealed. 1 ml of nitrogen purged MMA is injected into the vessel using a syringe and the system is sealed [30]. Finally, the reaction vessel is kept at 60 °C for 48 h. At the end of the reaction viscosity of the medium has increased dramatically. The mixture is diluted with chloroform and is precipitated with methanol. Finally the product obtained is washed with $CHCl_3$ to remove ungrafted PMMA, if formed. The product obtained is dried in vacuum for two days.

To prepare the reduced graphene oxide-polymethyl methacylate(MG) 100 mg GOPMMA is dispersed in 100 ml water by sonication to obtain yellowish-brown color dispersion. 1 ml hydrazine hydrate solution is added to this solution and refluxed at 100 °C for 24 h [7]. The product is collected via washing with methanol and centrifugation for several times. The black solid is dried in vacuum for overnight to obtain reduced graphene oxide-PMMA which is abbreviated as MG thought the whole manuscript. Gravimetric analysis suggests that MG samples contain 50% graphene by weight. The synthesis of MG is summarized in a scheme (Scheme 1) and the characterization of intermediate products is presented in supplementary information (suppl. Figs. 1–3).

2.3. Composite preparation

To prepare the reduced graphene oxide-PMMA (MG)/PVDF composites, 250 mg PVDF is mixed with different amount of MG in 5 ml DMF and heated at 60 °C for 1 h following sonication for 30 min to make homogeneous solution. The evaporation of the solvent in a Petri disk at 60 °C gives films of the nanocomposites which are kept at 60 °C for three days in vacuum. The composites are designated as MG0.5, MG0.75, MG1, MG3, MG5 respectively, the numbers indicates the weight percent of MG in the composites.

2.4. Characterization

2.4.1. Microscopy

The atomic force microscopy (AFM) is conducted in the noncontact mode at a resonance frequency of the tip end of ~250 KHz. BIBG, MG and MG3 are dispersed in DMF (0.01 w/v) and then a film is cast on a fresh silicon wafer. The samples are dried on hot plate in air at 60 °C and finally in vacuum at 60 °C for three days. The morphology of the dried films are studied using atomic force microscope (Veeco, model AP 0100).

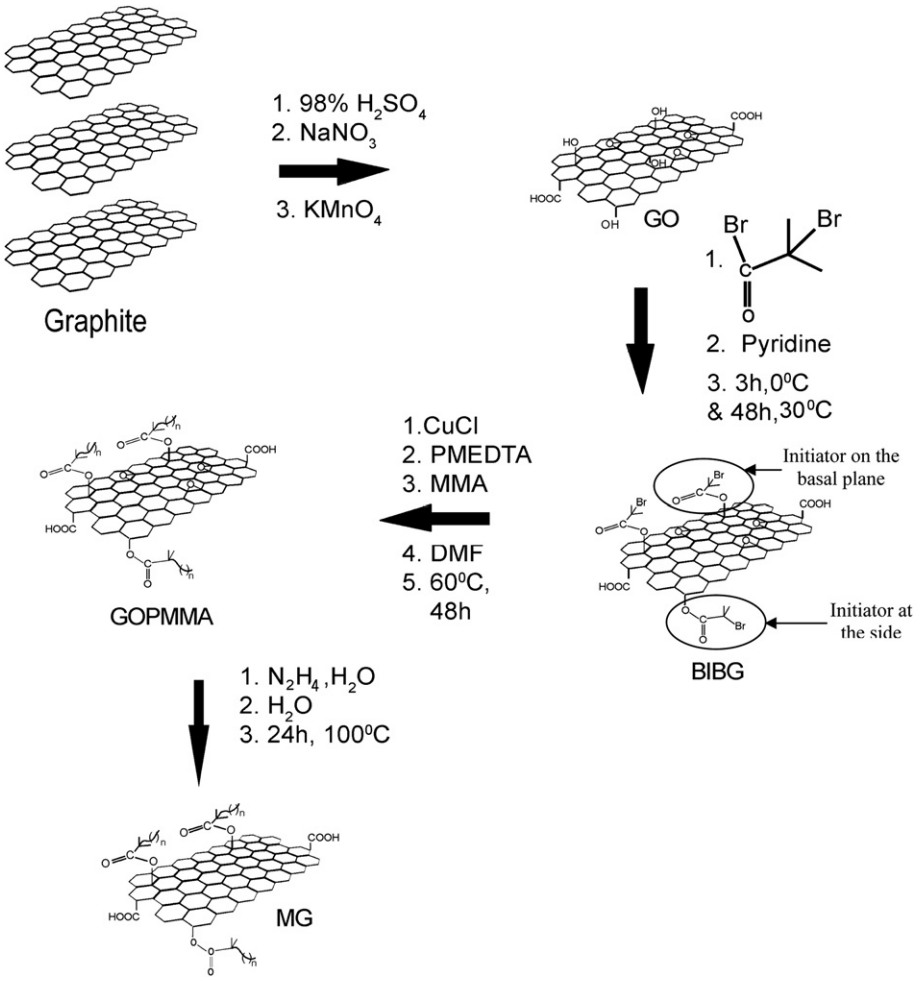

Scheme 1. Reaction scheme for the preparation of PMMA modified graphene (MG).

2.4.2. FTIR spectroscopy

FTIR study of the nanocomposite films is performed using FTIR (model 8400S Shimadzu) instrument. The nanocomposite films are cast from DMF solution (5% w/v) by spreading over the silicon wafer surface. The films are dried on a hot plate (60 °C) in air and finally in vacuum at 60 °C for three days.

2.4.3. X-ray scattering

XRD patterns of the nanocomposite films is obtained by fixing the nanocomposite film on an aluminum holder and the experiment is carried out using a Bruker AXS diffractometer (model D8) using Lynx Eye detector. The instrument is operated at 40 kV and 40 mA current. The samples are scanned from $2\theta = 5$ to 35° at the scan rate 0.5 s per step with a stepsize of 0.02 .

2.5. Thermal study

A Perkin–Elmer differential scanning calorimeter (Diamond DSC7) working under nitrogen atmosphere is used to measure the thermal property of the nanocomposite films. It is calibrated with indium before use. The samples are taken in aluminum pans and are crimped using a universal crimper. The samples are melted at 230 °C where they are kept for 5 min and then cooled to −30 °C at the scan rate of 5 °C/min. After keeping at −30 °C for 10 min the melt-cooled samples are heated at the rate of 40 °C/min to 230 °C. The higher heating rate is chosen to avoid melt-recrystallization of PVDF.

The thermal stability of the nanocomposites is measured using a Perkin–Elmer TGA instrument (Pyris Diamond TG/DTA) under nitrogen atmosphere at a heating rate of 10 °C/min.

2.6. Mechanical properties

The storage modulus (G′) and loss modulus (G″) and tanδ values of the nanocomposites are measured using a dynamic mechanical analyzer (DMA) (model Q-800, TA instruments). Samples are prepared in the film form (25 mm × 5 mm × 0.15 mm) by pouring the DMF solution on a die and evaporating it in air at 60 °C and finally in vacuum at 60 °C for three days. The films are then installed at the tension clamp of a calibrated instrument. The samples are heated from −100 to 130 °C at the heating rate of 10 °C/min. The G′, G″ and tanδ values are measured at a constant frequency of 1 Hz with a static force of 0.02 N.

Tensile tests are carried out from DMF cast films of uniform thickness using a universal testing machine (Zwick Roell, model Z005) at a strain rate of 1 mm/min at room temperature (30 °C). Each experiment is repeated for three times to observe reproducibility.

2.7. Conductivity measurement

The dc-conductivity of the film samples are measured by taking the samples between the two gold electrodes. The area of the samples and the thickness of the samples are measured by a screw

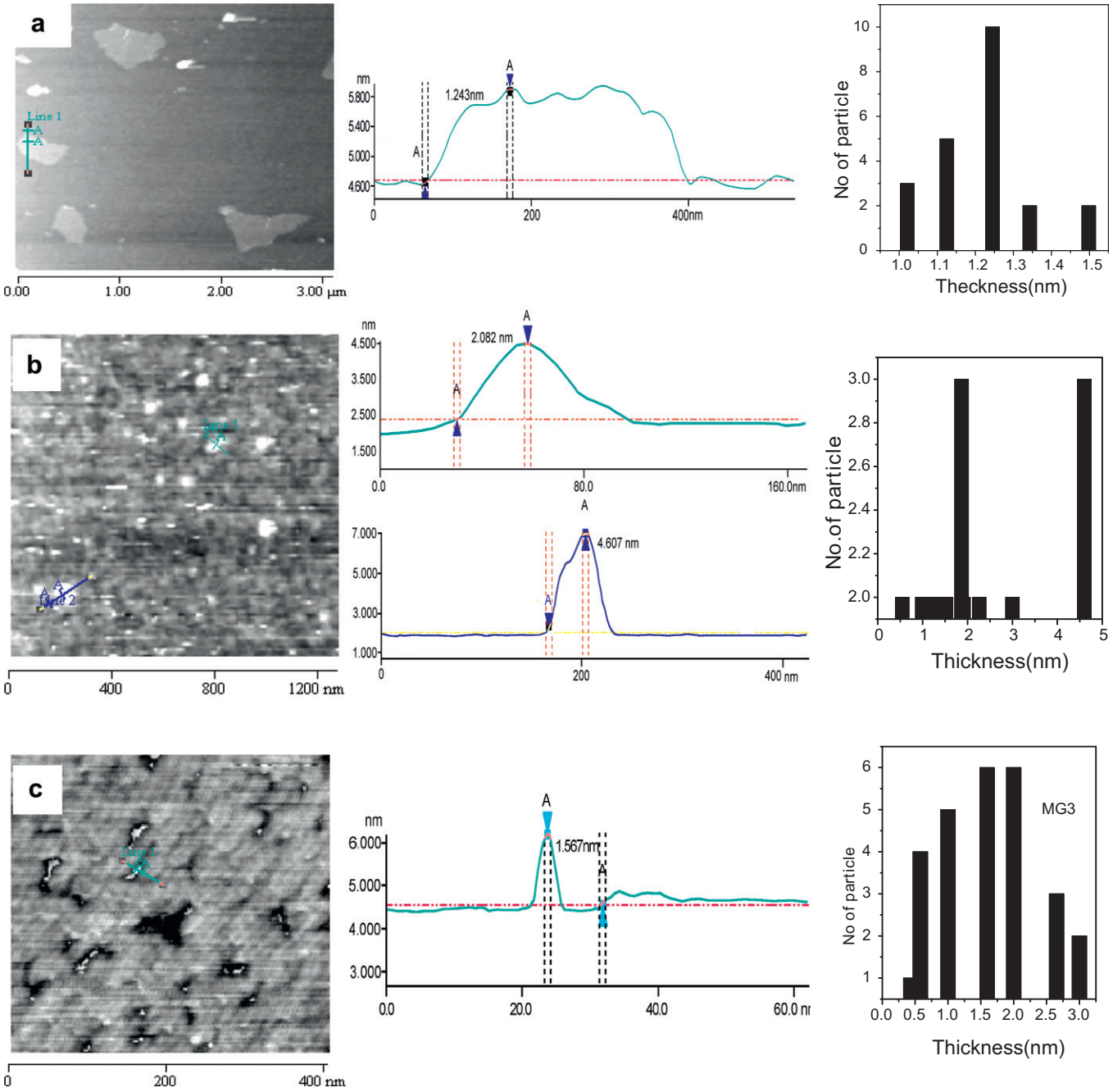

Fig. 1. Tapping mode AFM images and height profile of BIBG (a), MG(b), and MG3(c) and corresponding histogram at right side (obtained from ~30 objects).

gage. The conductivity (σ) of the film samples are measured by an electrometer (Keithley, model 617) by two probe technique at 30 °C using the equation:

$$\sigma = \frac{1}{R} \times \frac{l}{a} \tag{1}$$

where '*l*' is the thickness and '*a*' is the area and '*R*' is the resistance of the sample. For conductivity measurement at different temperatures the gold coated sample is placed on a brass platform separating from it by a mica plate. A low-voltage heater and a thermocouple are inserted into the platform. Heater temperature is controlled using a SELEC PID500 controller and a dimmerstat. The sample holder is covered with a glass jar to avoid draft. The temperature is raised from 30 to 130 °C at an interval of 10 °C. After waiting for 2 min at each temperature for thermal equilibrium the resistance of the sample is measured with a Keithley electrometer (model 617) using two probe technique.

3. Result and discussion

3.1. Morphology

The AFM images with their height profiles for BIBG, MG, and MG3 composites are presented in Fig. 1. Granular morphology of the composites with sheet structure of graphene is evident from the AFM micrographs. From the figure it is apparent that in BIBG the most probable height of graphene sheet is 1.2 nm. On polymerization with MMA the height has increased to 2 nm and

4.5 nm for two major populations of MG. Two different sites of polymerization (side and basal planes of graphene) are probably responsible for the two different height distribution. The 2 nm height is probably arising for polymerization on the initiator at the side of the graphene sheet (Scheme 1) and PMMA thus produced make a coat over the graphene sheet increasing the thickness. The possible reason for the occurrence of 4.5 nm thickness is that MMA is polymerized from the initiator attached to the basal plane of graphene sheet. PMMA, thus produced, enters into the gallery of graphene sheets and increases the gallery spacing to yield 4.5 nm thickness. In the MG/PVDF composite (MG3) some different phenomenon occurs due to the specific interaction of PVDF with PMMA. Due to the attractive force of PMMA chains PVDF chains enter into the MG gallery and as more and more PVDF chains enter into the MG gallery, it becomes expanded reducing the cohesive force between the two graphene sheets. As a result, exfoliation of MG sheets occurs showing lower height of MG in the AFM (height) images. The entrance of PVDF chains therefore causes more exfoliation of MG sheets, so this type of blending technique is effective for the preparation of the graphene nanocomposites with thinner graphene sheets. Here it may be surmised that 2 nm height population of MG breaks into 0.5, 1 and 1.5 nm and 4.5 nm population becomes exfoliated into 3 nm and lower height population. The different heights of MG sheets are produced due to exfoliation at different levels of the graphene sheets during blending.

It is now necessary to compare the AFM data with those of the other graphene initator and graphene polymer systems reported in the literature [31,32], The BIBG has a thickness of 0.73 nm [31], which is lower than that of ours (1.2 nm) and this difference is due to the fact that GO is reduced by hydrazine before initiator attachment in the former case. The reduction decreases the gap of graphene layers because of reduction of epoxides & basal hydroxyl groups of GO and only the side −OH and −COOH groups remain undisturbed [7,31]. The graphene thickness has increased to 3 nm in polystyrene (PS) grafted graphene sheets due to the presence of PS interface layers of 1 mm thickness [31]. In our case this increase is 0.8 nm and 3.3 nm indicating increased gallery spacing due to polymerization from initiating centers at different locations discussed above. In poly(acrylic acid) or poly(acryl amide) grafted graphene system [32], the heights of GO and GO-polymer are similar to those of ours. On blending MG with PVDF the gallery spacing decreases due to exfoliation of graphene. Hence the AFM data supports that modified graphene layers become thinner due to incorporation of PVDF chains within the sheet facilitating exfoliation of the graphene sheets during composite formation.

3.2. FTIR spectra

The FTIR spectra of MG nanocomposite films cast from DMF are presented in Fig. 2. From the figure it is apparent that pure PVDF has peaks at 797, 613 and 530 cm^{-1} which are retained for MG0.5 and MG1 composites. This indicates the formation of α polymorph of PVDF in these samples. With increased MG concentration (>1%) the FTIR peaks of β-polymorph PVDF (1271, 839, 510 cm^{-1}) become prominent indicating that MG induces β polymorph formation of PVDF [33,34]. It is to be noted that the >C═O stretching peak of PMMA of MG shows peak broadening in MG3 and MG5 sample indicating interaction of >C═O group with $>CF_2$ group of PVDF [25], The 759 cm^{-1} peak of PVDF is due to the $>CF_2$ bending and skeletal CF−CH−CF bending which show a shift to higher energy due to restriction of vibration for interaction with PMMA in MG0.5 and MG1 samples. But a different observation is noted in MG3 and MG5 composites where the $>CF_2$ and the skeletal CF−CH−CF bending vibration become easily feasible. The different orientation (random or parallel) of the graphene gallery with composition might be the

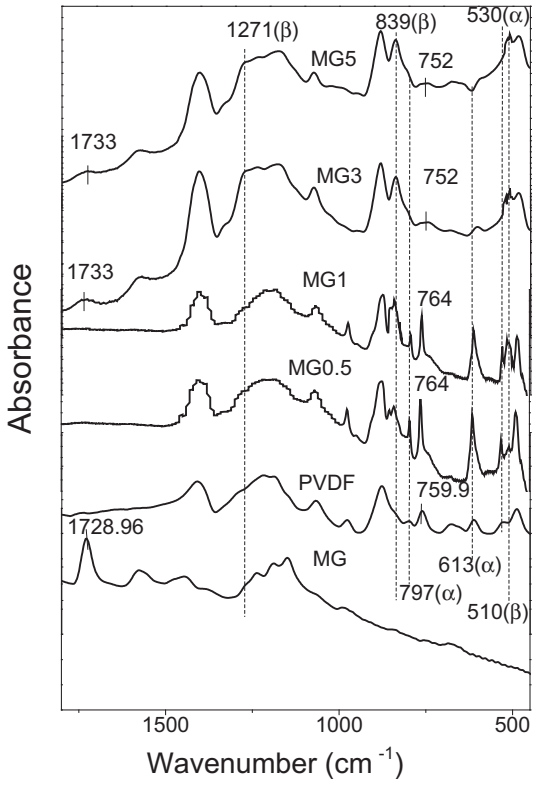

Fig. 2. FTIR spectra of MG and different PVDF-MG nanocomposites.

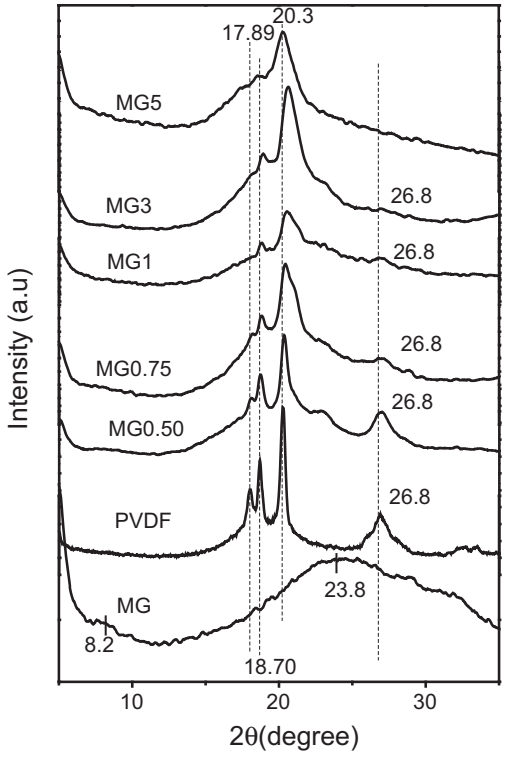

Fig. 3. WAXS patterns of MG and different PVDF-MG nanocomposites.

cause for such a difference in $>CF_2$/–CF–CH–CF– vibration frequency (cf. mechanical property).

3.3. WAXS pattern

In Fig. 3 the WAXS patterns of MG, PVDF and the MG-PVDF nanocomposites are presented. From the figure it is apparent that the MG is purely amorphous where as PVDF has α-polymorphic crystalline structure due to presence of diffraction peaks at $2\theta = 17.8$, 18.7, 20.3 and 26.8 [35,36]. It is to be noted that the relative intensity of 17.8, 18.8 and 26.8^0 peaks gradually decreases with increasing MG content in the sample suggesting increased concentration of β polymorph (characteristic diffraction peak at $2\theta = 20.3$) in the composite [35–38]. It is to be noted that in MG5 sample no characteristic diffraction peak of α PVDF is present and β polymorph is produced fully. So both from FTIR and WAXS study it may be concluded that graphene induce β polymorph formation of PVDF in the composite and it is complete for 5% MG content.

To understand the cause of β polymorph formation the potential energy (PE) calculation of Farmer et al. [39], and adsorption energy calculation of α and β polymorph of PVDF on carbon nanotube surface by Yu et al. [40], are used. It is evident from the PE calculation of Farmer et al. [39], that PE of β polymorph PVDF is higher by 0.15 eV for 5% H–H defect content PVDF sample. From the absorption energy calculation of Yu et al. [40], the average difference of adsorption energy between α and β polymorph PVDF on CNT surface is 0.21 eV. So it may be argued that during adsorption of PVDF on MG surface the energy barrier between the α polymorph and β polymorph may be overcome. This is possible because of the attraction of $>CF_2$ dipole by the >C=O group of grafted PMMA and orienting effect of graphene rings, causing an

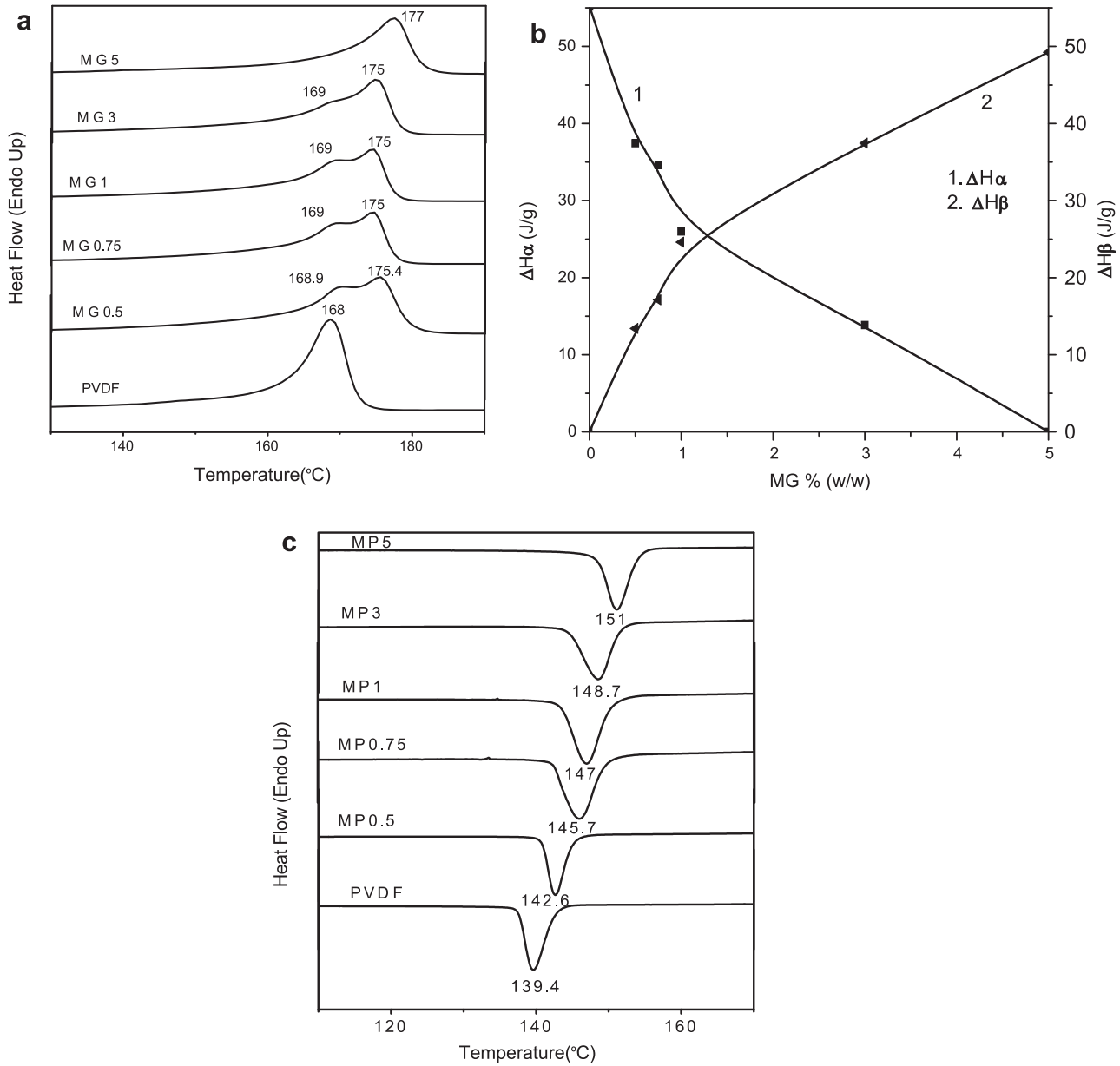

Fig. 4. (a) DSC melting endotherms (scan rate 40 °C/min) of different melt-cooled PVDF-MG nanocomposites. (b). Plot of enthalpy of α and β phases with MG content(w/w %) (obtained from thermograms of Fig. 4a). (c) DSC cooling endotherms (scan rate5 °C/min) of PVDF and different PVDF-MG nanocomposites.

extension of TGT$\overline{G}$ chain into TTTT conformation. So, during adsorption α-polymorphic chain with TGT$\overline{G}$ conformation may be transformed into all trans conformation of β polymorph PVDF and become adsorbed on the MG surface. Thus nucleation of β phase starts and the other chains crystallize in all trans conformation producing the β phase. The hundred percent formation of β phase in MG5 sample is due to the availability of sufficient MG surface area to the nucleating PVDF chains. The formation of mixture of α and β polymorph in the composite with lower MG concentration (<5%) is due to the lesser availability of MG surface for surface nucleation of PVDF chains rendering partial nucleation in α - polymorph.

3.4. Differential scanning calorimetry

In Fig. 4a, the DSC melting thermograms of melt-cooled samples are shown. The higher heating rate (40 °C/min) is chosen to avoid melt recrystallization [41,42]. The melt-cooled samples of PVDF show a single melting peak at 168 °C for the melting of α polymorph of PVDF. With addition of graphene another high temperature peak appears at 175 °C and this higher melting peak may be attributed to the melting of β phase PVDF. The DSC thermograms also support that in the 5% graphene sample β phase is produced fully. To quantify the formation of α and β phases the DSC thermograms are deconvoluted and areas are measured. It is evident from the Fig. 4b that there is a gradual decrease of ΔH of α phase PVDF with a concomitant rise of ΔH of β phase PVDF with increase of graphene content. The DSC cooling thermograms of the composite samples are presented in Fig. 4c and there is a gradual increase of crystallization temperature with increase of graphene content. Graphene sheets are therefore acting as nucleating agent by providing it's very large surface area for adsorption of PVDF chain and thereby causing easier nucleation.

3.5. Thermogravimetric analysis

In Fig. 5 the TGA thermograms of the MG-PVDF composites are presented. Pure PVDF degrades at 449 °C (determined from the first inflection point of the curve) but the composites have the degradation temperatures at 453, 462, 469, 471 °C for the MG0.5, MG1, MG3, MG5, respectively. So there is a significant rise in thermal stability of MG-PVDF composites. Only the 2.5% (w/w) graphene content of the samples (as 50% graphene is present in MG) causes an increase of degradation temperature of 21 °C. These results suggest that graphene acts as an effective thermal barrier due to its large aspect ratio and thereby hinders the degradation of PVDF. The better packing of all trans PVDF chains than that of TGT$\overline{G}$

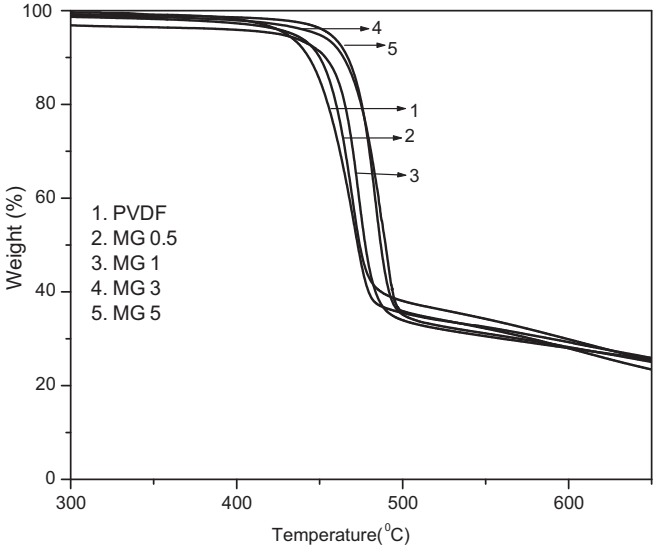

Fig. 5. TGA thermograms of PVDF and different PVDF-MG nanocomposites.

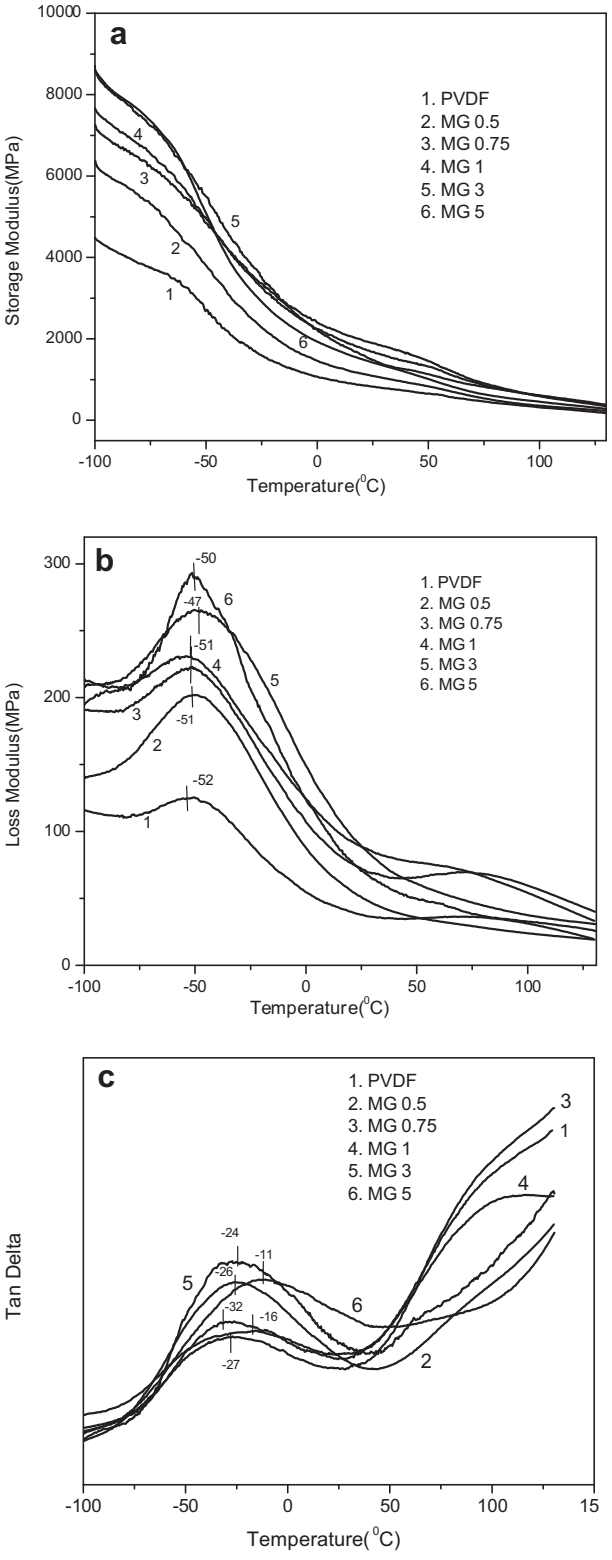

Fig. 6. Mechanical property–temperature plots of different PVDF-MG nanocomposites: (a) storage modulus, (b) loss modulus, and (c) tanδ.

chains might have some influence on the increased thermal stability [19]. This thermal stability enhancement is comparable to that of PVDF – multiwalled carbon nanotube composites [23].

3.6. Dynamic mechanical property

Fig. 6a–c shows the storage modulus (G′), loss modulus(G″) and tanδ plots with temperature for pure PVDF and MG-PVDF composites. The G′ relates the ability of the material to store energy when oscillatory force is applied and the G″ relates the ability to lose the energy. The storage modulus of the composites is much higher than that of the pure PVDF at the temperature range studied here. In the G′ vs T plot (Fig. 6a) there is a break at about −50 °C indicating a phase transition (glass transition) in the system. In the loss modulus plot (Fig. 6b) this glass transition is observed more distinctly and the transition temperature (T_g) may be computed from the peak temperature. It is evident from the figure and Table 1 that T_g data in the composite has increased by 4 °C only. The increase of T_g as obtained from the loss modulus data is not significant (Table 1). However, if one compute T_g data from the tanδ plot (Fig. 6c) the maximum increase of T_g in the present samples is 21 °C, a really significant increase for the composites. Also the values of T_g determined by the two methods differ from 20 to 37 °C for the pure PVDF and the composites. This is because of the difference of two techniques used for T_g measurement; one is related to the dissipation of energy as heat (loss modulus) and the other is related to the reduction of vibration of material, i.e. damping (tanδ). Graphene acting as a barrier for heat flow does not allow dissipation of heat significantly causing a very small decrease of T_g. On the other hand, increased stiffness of graphene composites (see below) causes damping variation to be very large and hence a large variation of T_g occurs in the composite with MG concentration from the tanδ plot. It is to be noted that there is a significant decrease in T_g for MG5 sample than that of MG3 sample. No definite reason can be afforded here.

It is evident from the Fig. 6a and b that storage modulus and loss modulus values are higher in the composites than that of pure PVDF. This indicates that the cause of G′ and G″ increase in the MG composites is the same and it is due to the reinforcement by the MG due to its high aspect ratio and good miscibility in the PVDF matrix. To get more distinct picture of the increase of G′ in the graphene composites compared to that of pure PVDF, the data are presented in Table 1 for different temperatures. It is evident from the table that the percent increase of storage modulus is maximum in the temperature range at the viscoelastic region (-50^0 to 0^0) where the movement of the polymer chain segments are relatively free so the reinforcement effect of graphene sheets are very large. The highest increase of G′ is 124% observed for the composite containing MG content of 0.75%(w/w) at 0 °C. At this low concentration the uniform dispersion and unidirectional distribution (see below) of graphene sheets may be the cause of the highest reinforcement.

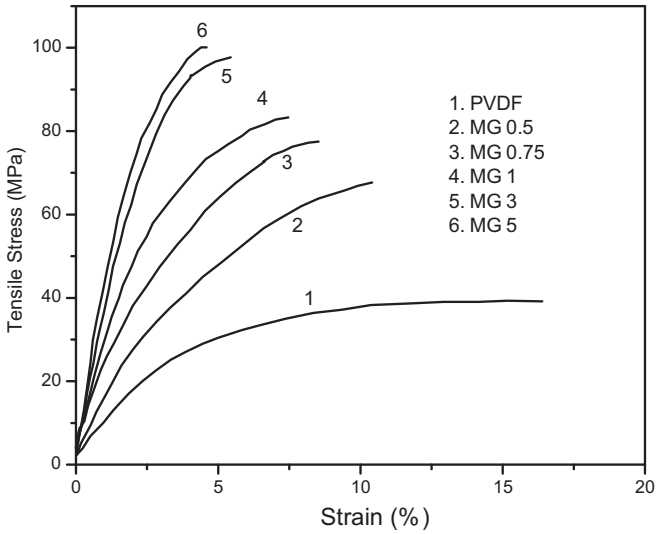

Fig. 7. Stress–strain curves of the pure PVDF and PVDF-MG nanocomposite films with different contents of modified graphene sheets.

It is now necessary to compare the data with the increase of storage modulus reported in the literature for this polymer. For PVDF clay nanocomposite the maximum increase in storage modulus is 100% [21,43]. For PVDF-Ag nanocomposite the highest increase is 67% [22], and that in multiwalled carbon nanotube it is 120% for 5%(w/w)concentration. So the graphene PVDF nanocomposite is more efficient in the reinforcement property than that of MWCNTs because lower concentration (0.75%) of MG produce the same maximum reinforcement property. Since in the MG there is 50% graphene so only 0.37% (w/w) graphene is sufficient to bring maximum increase in storage modulus. So graphene is a low cost and highly efficient biocompatible reinforcement material for PVDF than any other nanofiller.

3.7. Mechanical property

The stress–strain curves of PVDF graphene nanocomposites are presented in Fig. 7. It is evident from the figure that for a fixed value of strain there is an increase of tensile stress with addition of MG content. This indicates an increase in the stiffness of the film due to addition of MG. It is to be noted that the elongation at break gradually decreases with the increase of graphene content. The young's modulus, stress at break, strain at break and their percent increase with graphene content are presented in Table 2. The Young's modulus (Ey) of PVDF increases from 1.44 GPa to 6.07 GPa for 5% addition of modified graphene (MG) and the percent increase is quite high (321%) found at this composition. The stress at break also increases very dramatically from 39 to 100 MPa for 5%

Table 1
Summary of glass transition temperature(T_g) and storage modulus (G′) values of MG-PVDF nanocomposites measured by DMA.

Sample	T_g (°C)[a]	T_g (°C)[b]	G′ (MPa) at −100 °C	% increase	G′ (MPa) at −50 °C	% increase	G′ (MPa) at 0 °C	% increase	G′ (MPa) at 50 °C	% increase
PVDF	−52	−32	4481		2679		1068		653.3	
MG0.5	−51	−26	6374	42	3827	42	1458	36	829.9	25
MG0.75	−51	−27	7257	62	4852	81	2395	124	1453	120
MG1	−51	−16	7664	71	4984	86	2240	109	1319	100
MG3	−47	−12	8603	92	5126	91	1927	80	1011	53
MG5	−50	−24	8699	94	5527	106	2176	103	1129	71

[a] Measured from loss modulus plots.
[b] Measured from Tanδ plots.

(w/w) MG sample with a percent increase of 157%. In Fig. 8 the tensile stress and tensile strain values are plotted with MG concentration. Both the increase of tensile stress at break and the decrease in tensile strain are exponential with respect to MG concentration. This figure also suggests that 3% (w/w) MG concentration is sufficient to attain the leveling value of tensile strength and tensile strain indicating a rigidity percolation threshold at this composition. The toughness values presented in Table 2 shows a gradual decrease with increase of MG content.

In Fig. 9 the Young's modulus is plotted with MG content and initially its increase with MG content is slow then the increase is rapid at the concentration range 0.5–1% and finally the rate is slow resembling an autocatalytic (cooperative) behavior (inset). Such a large increase of young's modulus (E_y) and tensile strength (σ_S) is highest so far the results reported in literature [31,44,45]. In the polystyrene modified graphene–polystyrene composites a maximum increase of 70% and 57% in σ_S and E_y is observed, respectively [31]. This very large increase of σ_S and E_y in this composite may be attributed for the uniform dispersion of MG sheets in the composite due to blending.

Halpin and Tsai [46], derived an equation to calculate the effect of volume fraction of filler, relative modulus of the constituents and the reinforcement geometry of the composite moduli in a simple way and attempts are now made to explain the Young's modulus data of graphene composites with the help of the equation [44,45], Considering the random distribution of the MG in the composite, the modified form of the Halpin and Tsai equation may be written as [47–49];

$$E_\gamma = \left[\frac{3}{8}\frac{1+(2L_G/3T_G)\eta_L V_G}{1-\eta_L V_G}+\frac{5}{8}\frac{1+2\eta_T V_G}{1-\eta_T V_G}\right]E_P \quad (2)$$

Where

$$\eta_L = \frac{(E_G/E_P)-1}{(E_G/E_P)+(2L_G/3T_G)}$$

$$\eta_T = \frac{(E_G/E_P)-1}{(E_G/E_P)+2}$$

Where the E_Y, E_G and E_P are young's modulus of the composite, graphene and polymer respectively. L_G, T_G and V_G are the length, thickness and volume fraction of graphene units present in the composites [50]. For unidirectional (parallel) orientation of graphene nano sheets in the polymer films the modified Halpin–Tsai equation is represented by the equation :

$$E''_Y = \left[\frac{1+(2L_G/3T_G)\eta_L V_G}{1-\eta_L V_G}\right] \quad (3)$$

From the Fig. 9 it is evident that the experimental E_y values lie between the two theoretical curves drawn assuming random and unidirectional distribution. A careful analysis of the experimental

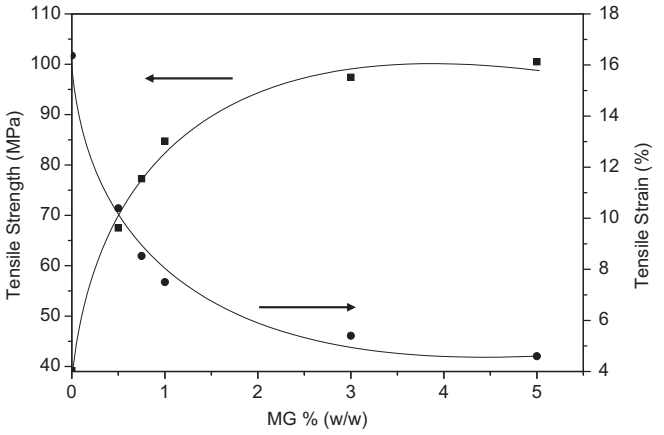

Fig. 8. Mechanical properties of PVDF-MG nanocomposite films with different MG contents: tensile strength (left) and elongation at break (right) versus graphene loading.

E_y data indicate that at low concentration of graphene it is close to the unidirectional (parallel) orientation but at high graphene concentration (≥1 %v/v) it is close to random orientation. A possible explanation for the parallel orientation in the low MG content sample is that due to directional nature of specific interaction between PVDF and PMMA at lower MG concentration orientation the MG sheets is unidirectional (parallel to the film). As the MG concentration increases the interaction of PVDF on large number of MG sheets looses its directional character and becomes isotropic. This causes a random distribution of MG sheets in higher concentrated MG composites. The experimental E_y curve suggests that the transition from parallel to random orientation of graphene sheets is cooperative in nature signifying that the directional character of interaction changes drastically by small increment of MG concentration in the composite.

3.8. dc-Conductivity

Fig. 10 shows the logσ vs $1/T$ plot of the MG5 composites and in the inset logσ vs composition plot is shown at 30 °C. Pure PVDF is an insulator having dc-conductivity of 5.3×10^{-13} s/cm and on addition of MG the dc-conductivity increases sharply showing a percolation threshold at 3.8%(w/w) MG concentration (containing actually 1.9 (w/w) % graphene). Thus the electrical percolation threshold (3.8%) is close to the mechanical percolation threshold (3%). The highest dc-conductivity (10^{-7} s/cm) is observed for the 20% MG sample at 30 °C. Temperature dependence of conductivity is studied for MG5, MG10 and MG20 samples (suppl. Fig. 4a and b) and conductivity increases with rise in temperature indicating the composites to behave as a semiconductor. To understand the conduction mechanism we have analyzed the data according to the equation of variable range hopping (VRH) model [51,52],

Table 2
Mechanical properties (stress, strain, modulus, toughness) of PVDF and PVDF-MG nanocomposites at 30 °C.

Sample	Strain at break	Stress at break (MPa)	% Increase of stress at break	Young's modulus (GPa)	% Increase of Young's modulus	Toughness (MPa)	% Decrease of toughness
PVDF	16.5	39.2	–	1.44	–	6278	–
MG0.5	10.5	67.3	71	2.25	77	5301	15
MG0.75	8.6	77.3	97	3.19	121	4914	22
MG1	7.5	82.9	111.3	4.04	180	5028	20
MG3	5.4	97.5	148.4	5.26	265	4210	33
MG5	4.6	100.7	156.5	6.07	321	3898	38

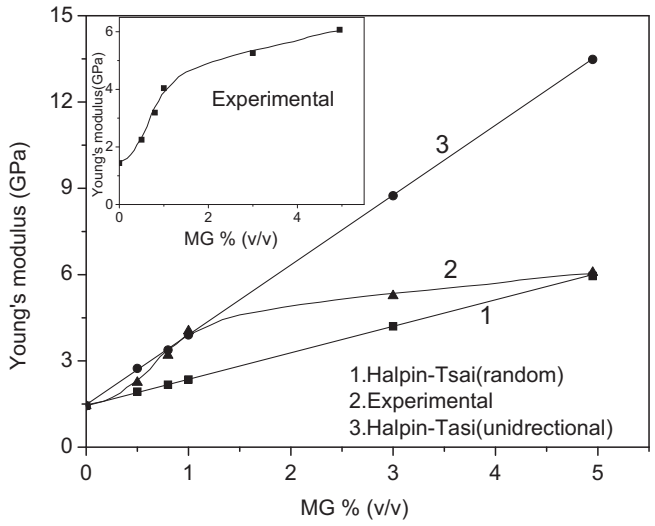

Fig. 9. Young's modulus vs volume % MG of the PVDF-MG nanocomposite films and Halpin–Tsai theoretical (random and unididirectional) plots.

$$\sigma = \sigma_0 \exp -(T_0/T)^{\gamma} \quad (4)$$

where σ is the dc-conductivity at a particular temperature(T), σ_0 is the pre-exponential factor and T_0 is a characteristic temperature and γ is a constant that depends on dimensionality of the process. The logarithmic variation of Eq. (1) can be expressed as

$$\ln W = \ln \gamma + \gamma \ln T_0 - \gamma \ln T \quad (5)$$

where $W = \delta \ln\sigma/\delta \ln T$. Thus a plot of ln$W$ vs ln$T$ should yield a straight line with a slope of γ. The ln$W$ vs ln$T$ plots are shown in Fig. 11 and in suppl. Fig. 5a and b where the slopes values are 0.80, 0.84 and 0.88 for MG5, MG10 and MG20, respectively. The T_0 values are obtained from the plots shown in the inset of Fig. 11 and suppl. Fig. 6a and b and they are 459, 439 and 622 K for MG5, MG10 and MG20, respectively. The present γ values are higher form any of 0.5, 0.33 and 0.25 values corresponding to any of three, two or one dimensional VRH model. In case of carbon black composites

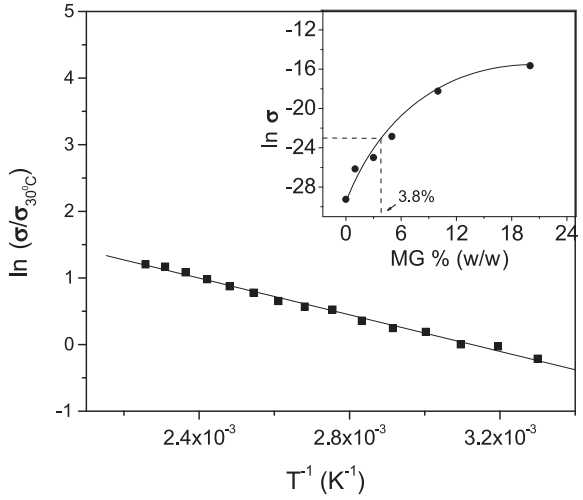

Fig. 10. Plot of lnσ/σ_{30} vs T^{-1} plot for MG 5 sample (inset lnσ vs MG loading showing percolation at 3.8% MG content).

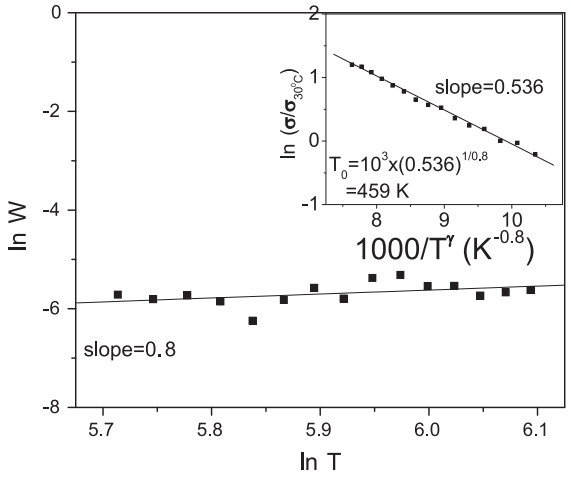

Fig. 11. Plot of ln$W$ vs ln$T$ and inset lnσ/σ_{30} vs $1000/T^{\gamma}$ plots for MG5 sample.

$\gamma = 0.66$ is attributed to super localization of wave functions on the carbon black network [53]. As the present γ values are even higher than 0.66 so it may be surmised that the conductivity is arising from the intergrain tunnelling and also from hopping between the grains [51].

4. Conclusion

The AFM data supports that PMMA increases the height of graphene sheet from 1.2 to 2 nm and 4.5 nm due to polymerization of MMA from initiators at side and at basal planes, respectively. MG layers become thinner due to exfoliation during composite formation from the incorporation of PVDF chains in the graphene gallery. FTIR and WAXS study indicate that graphene sheets influence the piezoelectric β-polymorph PVDF formation and it is complete for 5%(w/w) MG concentration. The nucleation of β polymorph is attributed from the adsorption energy of PVDF chains on graphene surface overcoming the energy barrier between the α and β polymorph. DSC study shows that the graphene sheets are nucleating agent for PVDF crystallization and there is a gradual decrease of ΔH of α phase PVDF with a concomitant rise of ΔH of β phase PVDF with increase of graphene content. There is a significant rise in thermal stability of MG-PVDF composites. The increase of T_g from loss modulus data though not significant, the T_g increase from the tanδ plot is really large (21 °C) signifying higher effect of damping in the composites than that of the heat loss from the composites. Storage modulus increases with increase in MG content and the highest increase of G′ is 124% which is comparable to that of PVDF-MWNT nanocomposites. The stress at break increases dramatically from 39 to 100 MPa for 5% (w/w) MG sample with a percent increase of 157% and the Young's modulus of PVDF increases from 1.44 to 6.07 GPa for 5% MG showing a highest percent increase (321%) yet reported in literature. Modified Halpin and Tsai equation has been used to calculate the effect of volume fraction of filler on the Young's modulus, taking both parallel and random distribution of graphene sheets in the composite film. The experimental results tally with the former at low graphene content and with the later for high graphene content (≥1 %v/v). The transition of parallel to random distribution is cooperative in nature signifying that the directional character of interaction changes drastically by small increment of MG in the composite. The composite exhibits electrical percolation threshold at 3.8% MG concentration and analysis of temperature dependent conductivity data indicate that the conductivity is arising from the intergrain tunnelling and also from hopping between the grains. So

a piezoelectric, conducting, biocompatible and high performance composite material suitable for different application is developed.

Acknowledgement

RKL acknowledges CSIR, New Delhi for granting fellowship.

Appendix. Supplementary material

Supplementary data associated with this article can be found, in the online version, at doi:10.1016/j.polymer.2010.09.067.

References

[1] Geim AK, Novoselov KS. Nat Mater 2007;6:183.
[2] Novoselov KS. Science 2004;306:666.
[3] Chen H, Muller MB, Gilmore KJ, Wallace GG, Li D. Adv Mater 2008;20:3557.
[4] Dragoman D. Appl Phys Lett 2007;91:203116.
[5] Nakajima T, Matsuo Y. Carbon 1994;32:469.
[6] Chen G, Wu D, Weng W, Wu C. Carbon 2003;41:579.
[7] Stankovich S, Dikin DA, Piner RD, Kohlhaas KA, Kleinhammes A, Jia Y, et al. Carbon 2007;45:1558.
[8] Pradhan SK, Nayak BB, Sahay SS, Mishra BK. Carbon 2009;47:2290.
[9] Gao W, Alemany LB, Ci L, Ajayan PM. Nat Chem 2009;1:403.
[10] Chung DDL. J Mater Sci 2002;37:1475.
[11] Stankovich S, Dikin AD, Dommett GHB, Kohlhaas KM, Zimney EJ, Stach EA, et al. Nature 2006;442:282.
[12] Stankovich S, Piner RD, Chen X, Wu N, Nguyen ST, Ruoff RS. J Mater Chem 2006;16:155.
[13] Ramanathan T, Abdala AA, Stankovich S, Dikin DA, Herrera-Alnso M, Piner RD, et al. Nat Nanotechnology 2008;3:327.
[14] Cote LJ, Cruz-Silva R, Huang J. J Am Chem Soc 2009;131:11027.
[15] Lu W, Weng J, Wu D, Wu C, Chen G. Mater Manuf Process 2006;21:167.
[16] Vickery LJ, Patil AJ, Mann S. Adv Mater 2009;21:2180.
[17] Tkalya E, Ghislandi M, Alekseev A, Koning C, Loos J. J Mater Chem 2010;20:3035.
[18] (a) Prasad KE, Das B, Maitra U, Ramamurty U, Rao CNR. PNAS 2009;106:13186;
(b) Kim H, Macosko CW. Macromolecules 2008;41:3317.
[19] Lovinger AJ. Development in crystalline polymers. London and New Jersey: Elsevier Applied Science; 1981.
[20] (a) Laroche G, Marois Y, Guidoin R, King MW, Martin L, Thein H, et al. J Biomed Mater Res 1995;29:1525;
(b) Ademovic Z, Gonera A, Mischnick P, Klee D. Biomacromolecules 2006;7:1429.
[21] Priya L, Jog JP. J Polym Sci B Polym Phys 2002;40:1682.
[22] Manna S, Batabyal SK, Nandi AK. J Phys Chem B 2006;110:12318.
[23] Manna S, Nandi AK. J Phys Chem C 2007;111:14670.
[24] Ansari S, Gianneliss EP. J Polym Sci B Polym Phys 2009;47:888.
[25] (a) Belke RE, Cabasso I. Polymer 1988;29:1831;
(b) Roerdink E, Challa G. Polymer 1980;21:1161.
[26] Park S, Jung I, Piner RD, An SJ, Li X, Velamakanni A, et al. Nano Lett 2009;9:1593.
[27] Nishi T, Wang TT. Macromolecules 1975;8:909.
[28] Samanta S, Chatterjee DP, Manna S, Mandal A, Garai A, Nandi AK. Macromolecules 2009;42:3112.
[29] Hummer WS, Offeman R. J Am Chem Soc 1958;80:1339.
[30] Kong H, Gao C, Yan D. J Am Chem Soc 2004;126:412.
[31] Fang M, Wang K, Lu H, Yang Y, Nutt S. J Mater Chem 2009;19:7098.
[32] Shen J, Hu Y, Li C, Qin C, Shi M, Ye M. Langmuir 2009;25:6122.
[33] Tashiro K, Kobayashi M. Phase Trans 1989;28:213.
[34] Cortili G, Zebri G. Spectrochem Acta 1967;23:2218.
[35] Lando JB, Doll WW. J Macromol Sci Phys 1968;B-2:205.
[36] Hasagawa R, Takahashi Y, Chatani Y, Tadokoro H. Polym J 1972;3:600.
[37] Bachmann MA, Lando JB. Macromolecules 1981;14:40.
[38] Guerra G, Karasz FE, MacKnight WJ. Macromolecules 1986;19:1935.
[39] Farmer BL, Hopfinger AJ, Lando JB. J Appl Phys 1972;43:4293.
[40] Yu S, Zheng W, Yu W, Zang Y, Jiang Q, Zhao Z. Macromolecules 2009;42:8870.
[41] Prest Jr WM, Luca DJ. J Appl Phys 1975;46:4136.
[42] Dikshit AK, Nandi AK. J Polym Sci Polym Phys Ed 2000;38:297.
[43] Patro TU, Mhalgi MV, Khakhar DV, Mishra AK. Polymer 2008;49:3486.
[44] Zhao X, Zhang Q, Chen D, Lu P. Macromolecules 2010;43:2357.
[45] Liang J, Hung Y, Zhang L, Wang Y, Ma Y, Guo T, et al. Adv Funct Mater 2009;19:1.
[46] Halpin JC, Kardos JL. Polym Eng Sci 1976;16:344.
[47] Mallik PK. Fiber-reinforced composites. N.Y; 1993. P-103.
[48] Zhang X, Liu T, Sreekumar TV, Kumar S, Merre VC, Hause RH, et al. Nano Lett 2003;3:1285.
[49] Qian D, Dickey EC, Andrews R, Rantell T. Appl Phys Lett 2002;81:5123.
[50] The L_G has been calculated from the measured length, breadth and thickness values of MG from the AFM data in the composite. As the above equation is derived for fibre/tubular morphology of the nanofiller so we calculated the effective length of graphene sheet from the measured average length, breadth and thickness data of the MG sheet in the MG3 composite. From the AFM data of MG3 sample the average length, breadth and thickness have values of 50 nm, 15 nm and 1.5 nm. Considering graphene platelet to be constituted of ten rectangular parallelepiped ($15/1.5 = 10$) contributing to a total length (L_G) of $50 \times 10 = 500$ nm and thickness (T_G) of 1.5 nm. V_G is calculated from the weights of graphene and PVDF in the composites taking (density (ρ) of PVDF 1.92 g/cm^3 and $\rho_{graphene} = 0.80$ gm/cm^3).
[51] Planes J, Wolter A, Cheguettine Y, Pron A, Genoud F, Nechtschein M. Phys Rev B 1998;58:7774.
[52] Yoon CO, Regu M, Moses D, Heeger AJ. Synth Metals 1994;63:47.
[53] Adriaanse LJ, Reedijk JA, Teunissen PAA, Brom HB, Michels MAJ, Brokken-Zipp JCM. Phys Rev Lett 1997;78:1755.